Article

Gas and Solution Uptake Properties of Graphene Oxide-Based Composite Materials: Organic vs. Inorganic Cross-Linkers

Mina Sabzevari [1], Duncan E. Cree [1],* and Lee D. Wilson [2],*

[1]   Department of Mechanical Engineering, University of Saskatchewan, 57 Campus Drive, Saskatoon, SK S7N 5A9, Canada
[2]   Department of Chemistry, University of Saskatchewan, 110 Science Place (Room 156 Thorvaldson Building), Saskatoon, SK S7N 5C9, Canada
*   Correspondence: duncan.cree@usask.ca (D.E.C.); lee.wilson@usask.ca (L.D.W.);
    Tel.: +1-306-966-3244 (D.E.C.); +1-306-966-2961 (L.D.W.)

check for updates

Abstract: This study focused on a comparison of the adsorption properties of graphene oxide (GO) and its composites that were prepared via cross-linking with chitosan (CTS) or Al^{3+} species, respectively. Comparative material characterization was achieved by several complementary methods: SEM, NMR spectroscopy, zeta-potential, dye-based adsorption, and gas adsorption at equilibrium and dynamic conditions. SEM, solids NMR, and zeta-potential results provided supporting evidence for cross-linking between GO and the respective cross-linker units. The zeta-potential of GO composites decreased upon cross-linking due to electrostatic interactions and charge neutralization. Equilibrium and kinetic adsorption profiles of the GO composites with methylene blue (MB) in aqueous media revealed superior uptake over pristine GO. The monolayer adsorption capacity ($mg\ g^{-1}$) of MB are listed in descending order for each material: GO–CTS (408.6) > GO–Al (351.4) > GO (267.1). The gas adsorption results showed parallel trends, where the surface area and pore structure of the composites exceeded that for GO due to *pillaring effects* upon cross-linking. The green strategy reported herein for the preparation of tunable GO-based composites revealed versatile adsorption properties for diverse heterogeneous adsorption processes.

Keywords: graphene oxide; chitosan; aluminum ion; cross-linking; gas uptake; composites

1. Introduction

Graphene oxide (GO) prepared from graphite is a promising material for large industrial scale fabrication of graphene [1–3]. The laminated GO structure has been known to be attractive for many technical applications, including dye removal from wastewater [4,5] energy storage, photovoltaics, and gas and humidity sensing [6–9], as well as gas capture [10–12]. Recent research on the interaction of GO laminated structures has revealed the potential utility of GO for various types of chemical separations in liquid and gas media [7,13].

The adsorption performance of modified GO sheets is promising, however, the uptake properties of GO sheets is not sufficient for large-scale practical applications because of the relatively low surface area (SA), porosity, and stability in aqueous media [14,15]. This can be attributed to the rearrangement of the graphitic structure of GO sheets after chemical modification via reduction and exfoliation treatments through chemical and thermal methods [14]. The limited interlayer sheet distance and low structural stability of layered GO limits its effective uptake properties toward target adsorbates in gas and aqueous media. Moreover, the shrinkage of framework materials caused by inadequate support

of the structure was estimated to render 50% of the accessible pore volume for adsorption-based applications [16].

In order to increase the adsorption performance and textural properties, the GO surface can be modified via cross-linking with organic and/or inorganic cross-linker units [17,18]. The tunable SA and pore structure (textural) of GO is understood due to cross-linking with the reactive oxygen containing groups on its sheet and basal plane domains [19–21]. GO-based composites and its cross-linked forms have been shown to be promising adsorbents toward various molecules [22–25]. Consequently, the use of appropriate cross-linkers such as chitosan or various metal ion species afford GO-based composites with hybrid properties that differ markedly from its precursors for adsorption-based applications. Thus, cross-linked GO framework materials often possess variable porosity, higher accessible SA, and greater adsorption capacity toward dye and gas species as compared with unmodified GO.

Chitosan is one of the most abundant modified natural polymers used for preparing hydrogels and multi-dimensional framework materials [26,27]. Cross-linking GO with chitosan or with metal ions has been reported to be an effective method to enhance the physical, chemical and mechanical properties of GO for various field applications [28–36].

Herein, we present a study on the preparation of GO-based composites cross-linked via organic (chitosan; CTS) and inorganic (Al^{3+}) species. The adsorption properties of GO-based composites are investigated in aqueous media with methylene blue (MB) and for gaseous species such as water and nitrogen. The goal of this study was to gain insight into the role of cross-linking and modification of GO by a systematic comparison of the adsorption properties of GO-based materials gas phase systems (H_2O vs. N_2) and a cationic dye probe in aqueous solution. This study will contribute to the development of GO-based adsorbents with enhanced adsorption properties and structural stability that will widen the field application of water treatment, greenhouse gas capture, dehumidification, gas sensing and storage [37]. Herein, it will be shown that cross-linked GO materials that contain chitosan display improved adsorption properties desired in advanced composites for chemical separations involving solid phase extraction (SPE) in both gas and liquid phase media.

2. Materials and Methods

2.1. Materials

Low molecular weight chitosan (M_w = 50,000–190,000 kDa, ~75%−85% deacetylation), aluminum nitrate nonahydrate ($Al(NO_3)_3 \cdot 9H_2O$), ACS grade sodium nitrite ($NaNO_3$), potassium permanganate ($KMnO_4$), sulfuric acid (98%, ACS grade), hydrogen peroxide (30% v/v) used in this study were purchased from Sigma-Aldrich Canada Ltd. (Oakville, ON, Canada). HPLC grade methanol was obtained from Fisher Scientific, Bridgewater, NJ, USA. Graphite flakes, natural, 325 mesh, 99.8% (metals basis) were provided by Alfa Aesar Thermo Fisher Scientific and purified prior to use with HPLC grade methanol to eliminate impurities.

2.2. Preparing Cross-Linked GO-Based Sorbents

First, GO powder was synthesized by oxidizing graphite powder using strong oxidants according to Hummer's method [38]. In this method, 4 g of graphite powder was mixed with 100 mL concentrated H_2SO_4 and added into a 500-mL flask contained in an ice bath. Then, 2 g of $NaNO_3$ was added to the mixture and stirred continuously for 4 h. After that, approximately 12 g of $KMnO_4$ was gradually added while the mixture was stirred for 2 h and the temperature was maintained below 10 °C. In the next stage, the mixture temperature was increased to 35 °C and stirred for 30 min. Subsequently, 240 mL of distilled water was slowly added to the mixture, which caused the temperature to rise to 90 °C. After stirring for 30 min at this temperature, 160 mL of water and 30% v/v H_2O_2 were added to terminate the reaction. The purification of the GO solution was conducted through multiple washings to remove residual chemicals. Finally, the GO paste was vacuum-dried at 40 °C to obtain dried GO powder.

The as-prepared GO was dispersed in water aided by sonication for 15 min. to yield a homogeneous GO dispersion in water. Then, the chitosan and Al nitrate solutions were prepared individually, by dissolving chitosan and $Al(NO_3)_3$ in 100 mL of glacial acetic acid (1% v/v) and Millipore water, respectively. The cross-linked GO sorbents were prepared by individual addition of aqueous chitosan (CTS) and aluminum salt drop-wise to each GO solution, respectively. The mixture was stirred continuously for 6 h followed by multiple washing and pH neutralization of the solutions under continuous stirring for an additional 12 h. The mixtures were dried at 295 K for 48 h to obtain the cross-linked GO composite powders. The sorbents prepared by this method at 1:6 w/w ratios of GO: cross-linker are designated GO–CTS and GO–Al.

2.3. Characterization

2.3.1. Scanning Electron Microscopy (SEM)

SEM images for the study of the morphology and porosity characteristics of GO-based sorbents were studied using a model SU8010 SEM (Hitachi, Tokyo, Japan) under an accelerating voltage of 3 kV.

2.3.2. ^{13}C and ^{27}Al Solid State NMR Spectroscopy

^{13}C solid state NMR experiments were performed using a Bruker AVANCE III HD spectrometer operating at 125.77 MHz (^{1}H frequency at 500.13 MHz) with a 4-mm DOTY NMR probe. The ^{13}C CP/TOSS (Cross Polarization with Total Suppression of Spinning Sidebands) NMR spectra were obtained with a spinning speed of 6 kHz, a ^{1}H 90° pulse of 5 µs with a fixed contact time (2 ms), and a ramp pulse on the ^{1}H channel. Data acquisition was accumulated (1200–2400 scans) with a recycle delay of 2 s. The ^{13}C MAS NMR spectra were acquired at a MAS rate of 11 kHz and a ^{13}C 90° pulse of 3.15 µs, variable scan accumulation (700–1024) with a recycle delay of 5 s. All ^{13}C experiments were recorded using 50 kHz SPINAL-64 decoupling during acquisition and all ^{13}C NMR chemical shifts (δ) were referenced to adamantane (δ = 38.48 ppm) for the low field signal.

The ^{27}Al MAS NMR experiments (frequency 130.32 MHz) were obtained at MAS spinning rates between 10 and 12 kHz and a 30 pulse width (1.4 µs) without ^{1}H decoupling. A variable number (200–400) of scans was accumulated with a recycle delay of 1 s, where the ^{27}Al chemical shifts were referenced to 1 M $Al(NO_3)_3$ aqueous solution (δ = 0 ppm).

2.3.3. Zeta-Potential Measurement

The surface charge (zeta potential) of the GO and GO-based solutions (0.01% *w/v*) were measured at different pH values using a Zetasizer Nano ZS (Nano ZS90, Malvern, UK), before and after cross-linking. All solutions containing powdered-samples were diluted to 0.01% *w/v* in Milli-Q water to estimate the zeta-potential.

2.3.4. Dye Sorption Studies

MB Adsorption Isotherms (Equilibrium Dye Uptake)

Adsorption properties of GO-based composite materials (GO–CTS and GO–Al) in aqueous media were studied and compared with GO by comparison of the uptake properties using MB at ca. pH 7. The optical absorbance of MB was studied to obtain the equilibrium MB uptake capacity of GO-based composite materials and their corresponding SA in aqueous solution using a batch mode method. The MB adsorption isotherms were obtained using a dosage of ~5 mg adsorbent added into 7 mL of MB solution at a variable initial dye concentration (C_o = 100–1000 µM). To achieve equilibrium, the samples were shaken on a horizontal shaker (SCILOGEX SK-O330-Pro, Rocky Hill, CT, USA) for 24 h. Next, the powdered samples were separated from the MB solution using low-speed centrifugation and the residual MB concentration (C_e) was measured using UV−vis spectroscopy (Varian Cary 100 Scan UV−vis spectrophotometer, Palo Alto, CA, USA) at λ = 664 nm. A linear calibration curve for the

MB optical absorbance from the slope (0.0616) = Abs 664 nm/[MB] using a 1-mM MB stock solution with appropriate dilution. The value of C_e obtained above enabled estimation of the MB equilibrium uptake (Q_e) by Equation (1).

$$Q_e = \frac{C_0 - C_e}{V} \cdot m \tag{1}$$

Q_e (mg g^{-1}) represents the MB adsorbed per unit mass of adsorbent, C_0 (mM) is the initial dye concentration, C_e (mM) is the residual amount of MB, V (L) is the volume of the MB solution, and m is the weight (g) of the adsorbent on a dry basis.

Dye adsorption using MB can be used as an effective method for estimation of the accessible SA of graphene-based materials [39]. After obtaining the monolayer adsorption capacity (Q_m) of the sorbent by a suitable isotherm model, the best-fit to the experimental results yields the corresponding sorbent SA according to Equation (2).

$$SA = Q_m \cdot N \cdot \delta \cdot Y^{-1} \tag{2}$$

Q_m (mol g^{-1}) refers to the maximum monolayer adsorption capacity at equilibrium per unit mass of sorbent, N (mol^{-1}) is Avogadro's number, δ represents the cross-sectional molecular surface area (m^2/molecule) occupied by MB ($\delta = 8.72 \times 10^{-19}$ when adsorbed in a "co-planar" orientation, while the dimensions of the MB are 1.43×0.61 nm^2 [40], and Y is the coverage factor, where Y = 2.0 for MB [41].

Kinetic Uptake Studies of MB (Kinetic Dye Uptake)

MB kinetic uptake of GO-based cross-linked samples in aqueous solution was studied to obtain the sorption capacity of GO before and after cross-linking. Kinetic adsorption isotherms were obtained using a one-pot method developed for monitoring of kinetic processes in situ for finely powdered sorbent materials [42]. Briefly, a sealed and folded filter paper was used to hold ca. 100 mg of a powdered sample in a tea-bag configuration. Then, the tea-bag system was immersed in the aqueous dye solution (250 mL), where C_o (MB) = 5 µM. Aliquots of the MB solution were pipetted (3 mL) at variable time intervals during the kinetic profile. Then, the optical absorbance of the sample aliquots was quantified via UV−vis spectrophotometry (Varian Cary 100 Scan UV−vis spectrophotometer). The MB adsorption capacity (Q_t) of the adsorbent at variable times (t) for the GO and GO–CTS materials was calculated using Equation (3) and obtained by plotting Q_t against variable time (t).

$$Q_t = \frac{C_0 - C_t}{m} \cdot V \tag{3}$$

C_0 and C_t refer to the MB concentration at t = 0 and variable time (t), respectively, V is the volume of the MB solution, and m is the weight of the sorbent in the tea-bag.

The adsorption kinetics and characteristics of GO and its cross-linked forms can be fit to the pseudo-first-order (PFO) and pseudo-second-order (PSO) models, where the best-fit parameters were obtained from the best-fit results of the corresponding model equation. The PSO model is defined by Equation (4), where the corresponding kinetic parameters (k_2 and Q_e) can be deduced from the best-fit isotherm results.

$$Q_t = \frac{Q_e^2 k_2 t}{1 + k_2 t Q_e} \tag{4}$$

Q_t is the amount of solute adsorbed by the sorbent at time t (mg g^{-1}), Q_e refers to the adsorbed amount of solute by the adsorbent (mg g^{-1}) at pseudo-equilibrium conditions, and k_2 is the rate constant according to the PSO adsorption model [42].

2.3.5. Gas Sorption Studies

Water Vapor Adsorption Isotherms

The Intelligent Gravimetric Analyzer (IGA) system, IGA-002 (Hiden Isochema, Warrington, UK) was used to investigate water vapor adsorption isotherms of samples where 30 mg of the adsorbent was put into a stainless-steel chamber attached to a microbalance under ultra-high vacuum conditions. The reactor temperature was controlled using a water bath and the samples were dried at 60 °C in vacuum (ca. 10^{-8} mbar) for 5 h. The IGA system affords a desired partial pressure in the chamber by adjusting the input and output valves. Once the sample mass has reached equilibrium within one partial pressure (mbar) value, the IGA system advanced to a higher partial pressure isotherm in the range between 0 to 30 mbar.

The corresponding SA (m^2/g) of the GO-based sorbents in the gas phase was calculated according to the obtained Q_m isotherm value for water vapor by Equation (5).

$$SA = Q_m \cdot N \cdot \delta \cdot M^{-1} \tag{5}$$

Q_m (g g^{-1}) is the maximum monolayer adsorption capacity at equilibrium condition per unit mass of sorbent, N (mol^{-1}) represents Avogadro's number, δ is the cross-sectional molecular area occupied by water vapor (m^2/molecule), where $\delta = 1.08 \times 10^{-19}$ for water vapor, and M (g mol^{-1}) is the relative molecular mass (M = 18.01) for water [43]. The pore volume of samples was estimated from the amount of gas adsorbed at p/p$_0$ = 0.99, where all pores become filled by water vapor and are assumed to exist as cylindrical-shaped pores.

Nitrogen Adsorption–Desorption Isotherms

The specific SA, pore size distribution and pore volume of GO and GO-based composite materials were estimated from nitrogen (N_2) gas sorption results using a Micromeritics ASAP 2020 (Norcross, GA, USA) instrument. All samples were degassed near 100 °C with an evacuation rate of 5 mmHg/s prior to conducting the gas uptake measurements. The Brunauer–Emmett–Teller (BET) SA of samples were obtained from the adsorption isotherm profiles of nitrogen gas (0.162 nm^2/molecule) [44]. The BET and the Barrett–Joyner–Halenda (BJH) methods were used to estimate the SA and pore volume of the sorbent material, respectively [45].

3. Results and Discussion

As indicated in Section 1, a comparative study of the role of cross-linker species (CTS, Al^{3+}) for the cross-linking of GO is required. While the use of cross-linkers described herein is reported in isolated studies [28–33,36,46], there is a need to examine the adsorption properties of such GO-based composites in a systematic fashion using complementary methods. Thus, a complementary materials characterization of the cross-linked GO composites was carried out to gain further insight on the role of these cross-linkers in such GO composites at fixed composition and the role of cross-linking on the adsorption properties toward gaseous adsorbates (H_2O, N_2), along with a model dye (MB) in aqueous media. The results for the SEM, solids NMR spectroscopy, zeta-potential, dye-based adsorption, and gas adsorption methods were obtained at equilibrium and dynamic conditions, as described in further details below.

3.1. Morphology of GO-Based Sorbents

The morphology and porosity characteristics of GO and its cross-linked forms were characterized using SEM. As evidenced in Figure 1a, the SEM image of GO revealed a denser layered-structure when compared to its cross-linked forms [14]. The GO-based sorbents (GO–CTS and GO–Al) in Figure 1a,b possess a layered-structure that appeared to consist of several two-dimensional GO sheets, in agreement with another report [46]. The cross-linking of GO sheets with chitosan and Al^{3+} ions

resembled a network-like layered structure. In the case of the GO–CTS (Figure 1b), the layers became slightly thinner since they contain pores within the sheets, as compared with cross-linked GO–Al (Figure 1c).
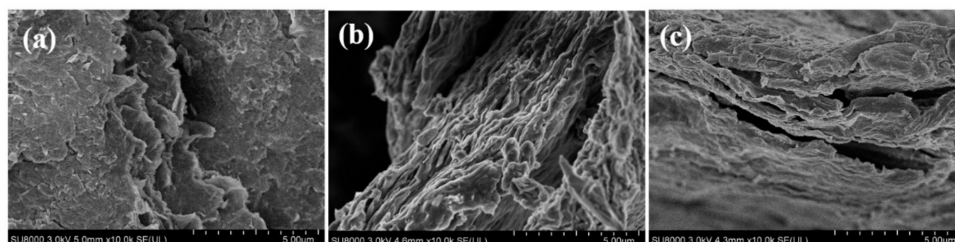

Figure 1. Scanning electron microscopy (SEM) micrographs of GO and the GO-based sorbents: (**a**) GO, (**b**) GO–CTS, and (**c**) GO–Al.

3.2. Chemical Characterization of GO-Based Composites

In Figure 2a, the ^{13}C NMR spectra for pristine GO exhibited three spectral lines that relate to carbon signatures of the epoxide groups (~60 ppm), hydroxyl groups (~70 ppm), and graphenic units (~130 ppm), in agreement with a previous report, [47] where the signatures in the 20–80 ppm range relate to the alkyl and alkenic groups. The main spectral lines for the GO–CTS composites were attributed to the broadening and shifting of the GO hydroxyl groups at ca. 70 ppm. In addition, the appearance of new ^{13}C spectral signatures (ca. 30 ppm and 100 ppm) were related to the glucosamine and acetylated forms of chitosan indicated in the ^{13}C spectra. Additionally, the presence of ^{13}C signatures at ca. 170–180 ppm concur with the presence of acetyl/amide groups of chitosan and the –COOH groups of GO. These signatures for the GO cross-linked material with chitosan relate to the presence of at least two chemically distinct carbonyl groups (amide and acetyl). Therefore, the variation in the ^{13}C NMR results between GO and GO–CTS supports the formation of cross-links between GO and chitosan in the composites, in agreement with ^{13}C NMR spectral results reported by Mahaninia and Wilson [48] for unmodified and cross-linked chitosan materials with various bifunctional linker systems.
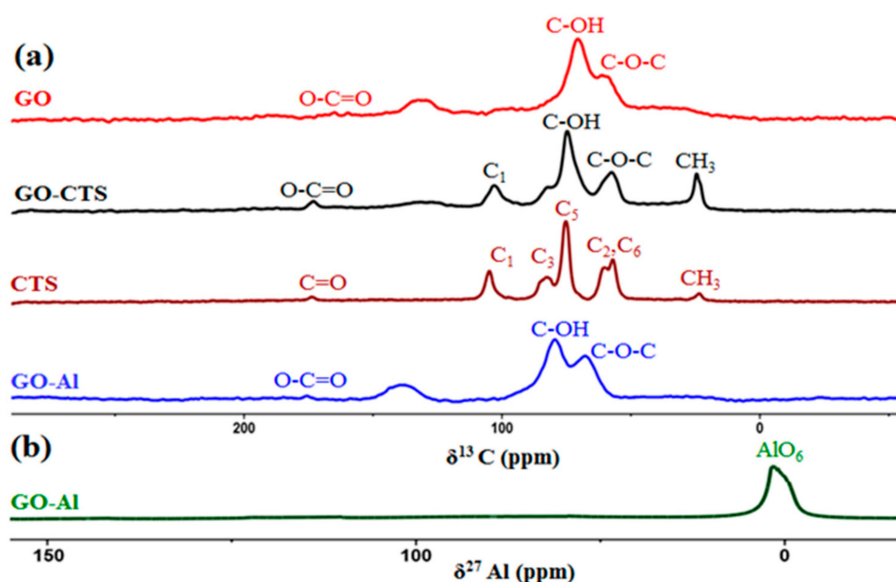

Figure 2. (**a**) Normalized ^{13}C and ^{27}Al solids NMR spectra of GO, chitosan and GO-based cross-linked composite (GO–CTS), and (**b**) ^{27}Al NMR spectrum of GO–Al.

Similarly, the ^{13}C NMR spectra for GO cross-linked with Al^{3+} ions (Figure 2b) showed broadening of the GO epoxide and hydroxyl groups (ca. 60 and 70 ppm) along with slight shifting of the ^{13}C

NMR lines. Additionally, the appearance of unique spectral signatures (ca. 160–170 ppm) noted upon cross-linking is related to the carbonyl groups and cross-linking between the polar functional groups (–COOH, –OH, etc.) of GO with Al^{3+} ions. Moreover, the appearance of ^{27}Al spectral signatures ca. 0 ppm in the ^{27}Al NMR spectrum relates to the presence of coordinated aluminum and residual Al $(NO_3)_3$, where these features provide support for cross-linking of the GO–Al composites [49]. The results reported herein represent a first example of the ^{13}C and ^{27}Al solid state NMR spectra for such GO-based composite materials.

3.3. Surface Charge

The zeta potential (ζ) values provide insight related to the nature of electrostatic bonding between the graphene surface of the GO-based samples and bound adsorbate species with variable electrostatic potential. Also, the magnitude of the point of zero charge (PZC) for the GO-based composite materials reflects the nature of the adsorptive interactions. The surface charge of the adsorbent phase (GO and GO-based composites) is influenced by the adsorption tendency and capacity from aqueous solution that contains the MB cation. Similarly, the uptake of gas species with variable polarity (N_2 vs. H_2O) is likely to affect the PZC of the adsorbent-gas system. The ζ-value for pristine GO (Figure 3) revealed a highly negative value (ζ below −30 mV) in its pristine form prior to cross-linking. This negative charge is mainly due to the polar and ionizing functional groups (–COOH and –OH) on the surface of GO sheets upon oxidation of graphite [50]. The ionization of –COOH and phenol (–OH) groups of GO may induce a stable colloidal suspension of GO sheets in polar solvents (such as water) due to favorable solvation and repulsive forces between the GO sheets [51]. The presence of such –OH and –COOH groups affords reactive sites for cross-linking of individual GO sheets with potential cross-linkers in aqueous media. As shown in Figure 3, the surface charge of unmodified GO was negative (−36.5 mV) prior to cross-linking. By contrast, the ζ-value was less negative for GO–CTS (−7.2 mV) and GO–Al (−3.6 mV) composite materials. The observed variation in the ζ-values upon cross-linking of the GO-based composites provides support that cross-linking of the surface functional groups of GO occurred. Electrostatic interactions between the positively charged ammonium sites of chitosan with the negatively charged sites of GO can lower the overall surface charge to yield a stable GO–CTS composite [29,52]. According to the ζ-value results for the GO sheets, it is expected that GO and its cross-linked forms (GO–Al and GO–CTS) will exhibit promising affinity toward cationic dye species such as MB across a wide range of pH values, especially near pH 7.
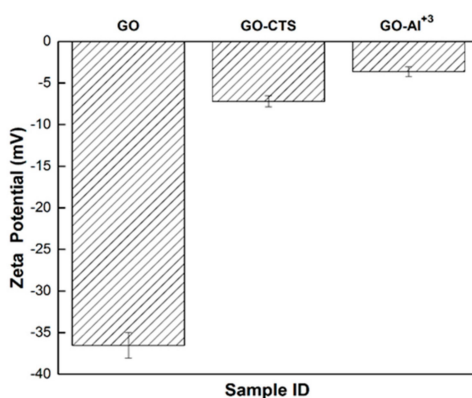

Figure 3. The ζ potential for GO-cross-linked composites at pH ~6 and 295 K.

3.4. Dye Sorption

Dye-based adsorption methods have been reported for the study of cellulose biopolymers and carbonaceous materials [53,54]. The adsorption performance and corresponding SA of the GO-based materials in aqueous media were studied by evaluating the MB uptake equilibrium and kinetic

conditions (cf. Figure 4a,b). The estimated SA in aqueous media for the GO materials was estimated by Equation (2) by use of the best-fit isotherm parameters derived from the dye uptake profiles.
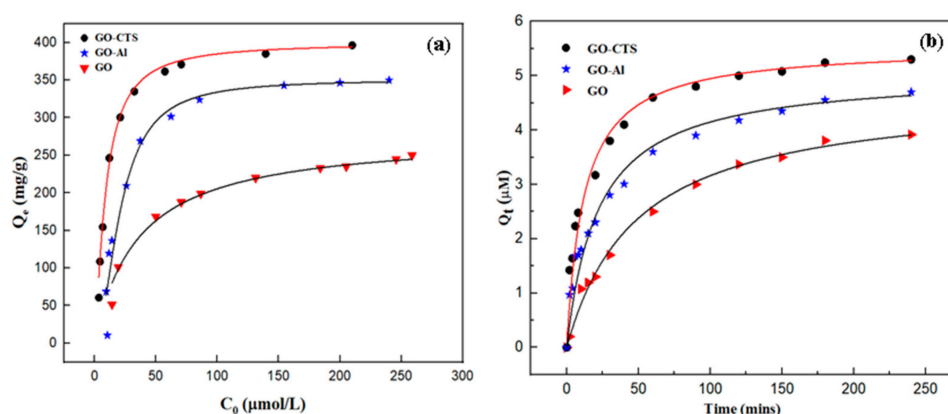

Figure 4. Methylene blue (MB) uptake profiles with GO and GO-based sorbents at pH ~6 and 295 K: (**a**) equilibrium isotherm, and (**b**) kinetic profiles. The fitted lines correspond to the Sips isotherm and pseudo-second-order (PSO) kinetic model, respectively.

3.4.1. Equilibrium Uptake of MB

The MB equilibrium absorbance was used to estimate the uptake properties of GO and GO-based composites. Greater decolorization of MB in solution occurs during the adsorption process according to higher MB uptake of the sorbents (GO, GO–CTS and GO–Al) at pH ~6. The unique MB adsorption isotherms and monolayer uptake capacity (Q_m) for the various sorbents are shown in Figure 4a.

The MB adsorption isotherms were analyzed by fitting the MB adsorption isotherm results at variable dye concentrations, where the best-fit sorption parameters were obtained by the Sips model (Equation (6)), according to correlation coefficients (R^2) near unity in Table 1.

$$Q_e = \frac{Q_m K_s C_e^{n_s}}{1 + K_s C_e^{n_s}} \tag{6}$$

Table 1. Sips and PSO adsorption isotherm parameters for GO-based composites with MB at pH 6 and 295 K.

		Sorbent		
Adsorbate	**Parameter**	**GO**	**GO-CTS**	**GO-Al**
Equilibrium	Q_m (mg·g^{-1})	267.1	408.7	351.4
	K_s (L·mg^{-1})	0.02811	0.1112	0.04714
	n_s	1.101	1.341	1.904
	R^2	0.9660	0.9781	0.9760
	SA (m^2·g^{-1})	235.7	335.5	288.5
Kinetic	Q_m (μmol·g^{-1})	4.170	5.541	5.059
	k_{pso} (g·μmol·min^{-1})	0.00435	0.015	0.010
	R^2	0.994	0.979	0.976

At equilibrium conditions, Q_e and Q_m refer to dye uptake at non-saturative and monolayer saturation conditions, respectively. K_s represents the Sips equilibrium adsorption constant that reflects adsorption energy contributions, C_e is the residual equilibrium dye concentration, and n_s indicates the surface heterogeneity of the sorbent. The GO-based sorbents had Q_m (mg/g) values listed in descending order, as follows: GO–CTS (408.7) > GO–Al (351.4) > GO (267.1). The monolayer adsorption capacity was higher for the GO-based composites (GO–CTS and GO–Al) over pristine GO. The trend relates to

cross-linking effects, where the presence of more accessible adsorption sites is favored at higher Q_m values for MB. Cross-linking of GO with chitosan and Al^{3+} species led to changes in the GO framework structure that favoured adsorptive interactions with MB. Moreover, the comparative ordering of Q_m values for MB uptake among the GO-based composites relates to the relative magnitude of the ζ-values for the various materials in aqueous media (cf. Figure 3). A comparison of GO–CTS with GO–Al materials revealed correlation between the trend in Q_m and ζ-values of the charged GO surfaces, where Q_m (GO–CTS) > Q_m (GO–Al). The greater Q_m values of GO–CTS relate to the greater number and relative accessibility of anionic sites of GO over the GO–Al composite. The more porous framework structure of the GO–CTS composite is supported by its greater pore volume, in agreement with the nitrogen adsorption results (vide supra), as compared with the GO–Al composite. As well, the use of chitosan as the cross-linking agent was reported to adsorb additional MB in solution via electrostatic interactions [55]. The dye-based SA estimates of the adsorbent materials were estimated using Q_m values obtained from the best-fit isotherm parameters listed in Table 1. The GO-based composites showed greater SA values as compared with pristine GO, where the MB uptake adopted the following order: GO–CTS > GO–Al > GO. This trend relates to the *pillaring effect* [56] between the GO sheets, where the variable interlayer spacing is governed by the cross-sectional diameter (*d*) of the cross-linker (*d*-CTS > *d*-Al^{3+}). While GO has relatively high SA in its dispersed form, it is known to undergo aggregation in aqueous solution due to hydrophobic effects, thereby lowering the MB uptake to surface coverage of GO to below monolayer saturative conditions [57]. Cross-linking serves to prevent such aggregation of GO sheets, thus stabilizing the GO framework that favors greater uptake of MB.

3.4.2. Kinetic Uptake of MB

Figure 4b represents the kinetic uptake profiles of GO and GO-based materials, where an increase in the MB uptake capacity for the sorbent occurred within 40 min followed by a reduced uptake thereafter up to 250 min. The greater initial rate of MB uptake below 40 min is attributed to the availability of negative surface sites on the sorbent for dye uptake. The lower rate of uptake (t > 40 min) relates to a reduction in the available surface sites as the adsorbent surface becomes saturated with dye species. The GO–CTS composite had greater MB uptake and more negatively charged surface sites (cf. ζ-value in Figure 3), while reduced MB uptake of the GO–Al composite concurs with its less negative ζ-value and pore volume.

The kinetic uptake results were analyzed using the PSO kinetic model [42,53,54], where good fits are evidenced by correlation coefficients (R^2) near unity ($0.976 \leq R^2 \leq 0.994$). Accordingly, the kinetic parameters (k_{pso} and Q_m) for GO–CTS and GO–Al materials revealed greater kinetic uptake of MB uptake versus pristine GO. The Q_m (μmol g^{-1}) values for the sorbents are listed in descending order: GO–CTS (5.54) > GO–Al (5.05) > GO (4.17). The PSO rate constants (k_{pso}; g/μmol. min) followed the same relative trends, as follows: GO–CTS (0.015) > GO–Al (0.010) > GO (0.004). The trend in Q_m and k_{pso} values parallels the trend for the role of cross-linking described for the equilibrium uptake results for MB outlined above.

The superior kinetic uptake of the composite materials provides support that synergistic effects may occur due to cross-linking between GO and the cross-linkers (CTS or Al^{3+}). Cross-linking of GO appears to increase the accessibility of the adsorption sites for MB uptake, in agreement with the trends for the kinetic and equilibrium adsorption parameters [56]. The MB uptake kinetics for the sorbent materials indicated the role of diffusion effects through the pore network, as shown by a reduced diffusion contribution as the contact time increased. This trend parallels the decreased number of available adsorption sites across the kinetic profile.

3.5. Gas Sorption

The gas uptake properties, porosity characteristics and specific SA of the GO materials were studied by comparing the solid–gas adsorption–desorption isotherms. The isotherm results for water (polar) and N_2 (nonpolar) gases are shown in Figures 5 and 6, respectively.
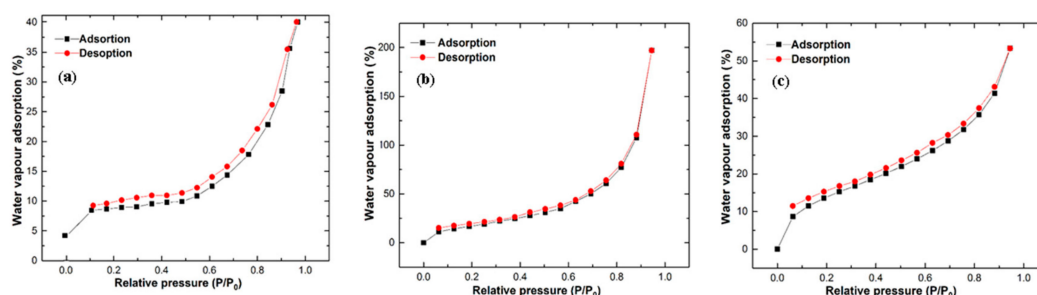
Figure 5. Water vapor adsorption and desorption profiles at 298 K: (**a**) pristine GO, (**b**) GO–Al composite, and the (**c**) GO–CTS composite.
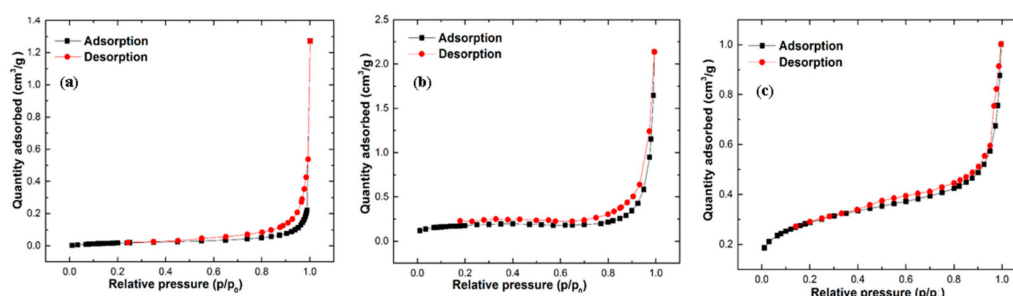

Figure 6. Nitrogen adsorption and desorption isotherm at 77 K: (**a**) pristine GO, (**b**) GO-Al composite, and the (**c**) GO–CTS composite.

3.5.1. Water Vapor Analysis

The water vapor adsorption–desorption isotherm results and the related gas sorption parameters for GO and its cross-linked composites are shown in Figure 5 and Table 2. The GO-based/water vapor systems displayed Type II isotherms for the desorption–adsorption profiles, as defined by the International Union of Pure and Applied Chemistry (IUPAC) classification system [58,59]. The adsorption of water vapor for the GO-based sorbents showed similar features related to the composite structure and the role of polar adsorption sites. In addition, the monolayer saturation in the adsorption profile occurred at a relatively low relative pressure (p/p_0) near 0.3, while a major fraction of vapor uptake occurred at $p/p_0 > 0.8$.

Table 2. Brunauer–Emmett–Teller (BET) adsorption isotherm parameters for GO and GO-based composites with water vapor at 298 K.

Adsorbate	Parameter	Sorbent		
		GO	**GO-CTS**	**GO-Al**
Water vapor	Q_m (mg/mg)	11.10	17.54	13.95
	SA (m^2/g)	408.9	560.9	481.8
	Pore volume (cm^3/g)	0.53	1.97	1.33

The water vapor adsorption (w/w %) for GO and its composites adopt the following trend: GO–CTS (198) > GO–Al > (54) > GO (41), where the GO composites surpass the relative uptake capacity of GO. This trend is in-line with the *pillaring effects* of the GO framework for the composites, and the modified surface sites and textural properties of GO upon cross-linking. The water vapor uptake of GO–CTS exceeds that of GO–Al composites, in parallel with the greater SA and pore volume of GO–CTS over GO–Al. The enhanced textural properties, such as the pore volume and presence of polar adsorption sites of the GO–CTS composite, facilitate greater diffusion of water vapor into the micropore domains of the cross-linked framework.

The SA and pore volume of the GO-based materials was estimated from the water vapor uptake profiles, exceeding the tabulated values of unmodified GO in Table 2. The GO–CTS composite had the highest water vapor uptake, in parallel agreement with the dye adsorption results. However, the SA values estimated from the water vapor isotherms were notably higher than values estimated from the dye adsorption isotherms. The offset in the adsorption parameters (Q_m and pore volume) for the liquid versus gaseous adsorbates relates to differences in their relative polarity and molecular size. In the case of small polar species such as water, greater micropore accessibility for water occurs for cross-linked GO, when compared against MB. The greater molar volume of MB over water, along with the respective differences in the relative polarity of each adsorbate, play a role in the electrostatic interaction with the GO active sites upon adsorption. The somewhat greater Q_m values in aqueous media and in the presence of water vapor for the GO–CTS and GO–Al sorbents provide support that water induces swelling in the GO-based materials, in contrast to adsorption of nitrogen gas.

The variable adsorptive affinity of the gaseous adsorbates further suggests the role of size effects and dipolar surface interactions in sorbent–gas systems. Notwithstanding the role of solvent swelling of the sorbents in aqueous solution for sorbent–dye adsorption processes, a comparison of the gas adsorption of GO-based materials with a nonpolar gas was studied using nitrogen gas as the adsorbate probe.

3.5.2. Nitrogen Adsorption–Desorption

The nitrogen adsorption–desorption isotherms of the GO-based materials are shown in Figure 6. The BET SA, pore size and pore volume (textural) properties of the sorbents were estimated from analysis of the N_2 adsorption isotherm results, as listed in Table 3. The nitrogen adsorption profiles for GO and GO-based composites follow a Type II isotherm profile [58]. The low N_2 uptake for GO indicates the limited interlayer spacing between the GO sheets, as evidenced by its more dense structure, thereby limiting its accessible pore volume, as supported by the SEM results in Figure 1. GO showed an increase in N_2 adsorption up to a value of p/p_0 near 0.7, where a hysteresis occurred for $p/p_0 > 0.8$ that provides support for mesopore domains in GO. The GO-based composites displayed greater N_2 uptake, where the major fraction of gas adsorption occurred at relatively low values of p/p_0, indicative of microporous materials. Cross-linked GO containing CTS or Al^{3+} ions yielded composite materials with an overall greater pore volume, where a hysteresis effect is noted with a negligible increase in the nitrogen adsorption which occurred up to a p/p_0 value near 0.8.

Table 3. BET adsorption isotherm parameters for GO and its composites with nitrogen at 77 K.

Adsorbate	Parameter	Sorbent		
		GO	GO-CTS	GO-Al
Nitrogen	SA (m²/g)	0.611	1.40	1.24
	Pore size (nm)	9.66	34.9	18.8
	Pore volume (cm³/g)	0.191	0.830	0.761

Comparison of the isotherms for GO and GO-based composites revealed differences between these materials, as evidenced by their variable textural properties. In general, cross-linked GO (GO–CTS and GO–Al) materials have greater pore structure, where GO–CTS samples have comparable size and volume (18.8 nm, 1.24 m² g^{-1}) relative to GO–Al (34.9 nm, 1.40 m² g^{-1}). The foregoing results showed parallel trends to the pore volume results for GO–CTS (0.83 cm³/g) versus GO–Al (0.76 cm³/g) that govern the greater nitrogen sorption at higher p/p_0 values. The nitrogen uptake capacity of cross-linked GO samples can be directly correlated to their similar textural properties in an anhydrous environment, in accordance with the role of solvent swelling [41,60]. The use of chitosan as a cross-linker unit yielded a slightly greater porosity (pore size and pore volume) and SA compared to GO–Al. The interconnected network structure between GO sheets in the GO–CTS composite afforded greater diffusion of polar adsorbates (MB and water vapor) over nitrogen, especially in the presence of H_2O due to solvent

swelling when CTS was the linker unit. Comparing the SA and sorption capacity of sorbent materials revealed a greater SA, pore volume and uptake of cross-linked GO samples. This phenomenon relates the role of *pillaring effects* of GO sheets upon cross-linking due to greater interlayer spacing and accessibility of the active adsorption sites for the GO composites.

These trends noted for gas adsorption of the GO-based materials are in-line with the uptake results for MB in aqueous media described above. This difference in uptake values by other species (MB and water vapor) is attributed to the weak surface interactions of GO and GO-based sorbents with nitrogen gas, where its greater molar volume over H_2O vapor is an important steric consideration, along with the role of dipolar interactions.

4. Conclusions

In this study, graphene oxide (GO) materials were prepared by cross-linking GO with CTS and Al^{3+} ions, respectively. The GO sorbent materials were characterized by several complementary methods, such as solid-state ^{13}C and ^{27}Al NMR spectroscopy and zeta potential results. The latter provided support that cross-linking altered the surface properties of GO upon cross-linking. The adsorption properties of GO and its composites were evaluated with two types of gases (N_2 and H_2O), along with adsorption properties in aqueous solution with a cationic dye (methylene blue; MB) to reveal differences in their SA and pore structure properties. The dye uptake properties for GO-based composites with MB revealed higher SA (m^2/g), as follows: GO–CTS (335.0) > GO–Al (288.5) > GO (235.7). The monolayer adsorption capacity (Q_m; mg/g) for the sorbents at equilibrium and under kinetic conditions revealed that GO–CTS composites possess the highest uptake among the sorbents studied herein. The cross-linking of GO with chitosan yields a 3D-framework with greater accessible SA, porosity and active sorption sites when compared with pristine GO. The improved textural properties of GO–CTS is supported by complementary water vapor uptake and dye adsorption in aqueous media. The gas uptake of GO and its composites toward molecular nitrogen are notably lower (cf. Table 3) relative to water vapor or MB in solution. The adsorption sites of GO composites have greater accessibility for processes that involve water in its condensed or vapor state, revealing the key role of hydration and solvent swelling effects versus anhydrous media. The cross-linkers (CTS or Al^{3+}) in such GO frameworks facilitate accessibility of the GO interlayer sites via *pillaring effects*, as evidenced by improved diffusion and uptake of adsorbates at the active sites for cross-linked GO. Herein, the role of cross-linking was demonstrated as an efficient and environmentally friendly method to tune the textural and sorption properties of GO for adsorption applications in solution and for gas phase systems. The reported improvements to the physicochemical properties of GO-based materials herein will contribute to the use of cross-linked GO for diverse adsorption-based applications: chemical separations, environmental remediation, and gas storage for energy production [61–64]. In particular, further studies are underway to evaluate the enhanced textural properties and mechanical strength of such composites for demanding adsorption-based processes under high pressure conditions for advanced technological applications.

References

1. Dreyer, D.R.; Todd, A.D.; Bielawski, C.W. Harnessing the Chemistry of Graphene Oxide. *Chem. Soc. Rev.* **2014**, *43*, 5288–5301. [CrossRef] [PubMed]
2. Safavi, A.; Tohidi, M.; Mahyari, F.A.; Shahbaazi, H. One-Pot Synthesis of Large Scale Graphene Nanosheets from Graphite-Liquid Crystal Composite via Thermal Treatment. *J. Mater. Chem.* **2012**, *9*, 3825–3831. [CrossRef]
3. Compton, O.C.; Nguyen, S.T. Graphene Oxide, Highly Reduced Graphene Oxide, and Graphene: Versatile Building Blocks for Carbon-Based Materials. *Small* **2010**, *6*, 711–723. [CrossRef] [PubMed]
4. Yang, S.T.; Chen, S.; Chang, Y.; Cao, A.; Liu, Y.; Wang, H. Removal of Methylene Blue from Aqueous Solution by Graphene Oxide. *J. Colloid Interface Sci.* **2011**, *359*, 24–29. [CrossRef] [PubMed]
5. Sun, H.; Cao, L.; Lu, L. Magnetite/Reduced Graphene Oxide Nanocomposites: One Step Solvothermal Synthesis and Use as a Novel Platform for Removal of Dye Pollutants. *Nano Res.* **2011**, *4*, 550–562. [CrossRef]
6. Basu, S.; Bhattacharyya, P. Recent Developments on Graphene and Graphene Oxide Based Solid State Gas Sensors. *Sens. Actuators B Chem.* **2012**, *173*, 1–23. [CrossRef]
7. Borini, S.; White, R.; Wei, D.; Astley, M.; Haque, S.; Spigone, E.; Harris, N.; Kivioja, J.; Ryhänen, T. Ultrafast Graphene Oxide Humidity Sensors. *ACS Nano* **2013**, *12*, 11166–11173. [CrossRef]
8. Sun, Y.; Wu, Q.; Shi, G. Graphene Based New Energy Materials. *Energy Environ. Sci.* **2011**, *4*, 1113–1132. [CrossRef]
9. Lightcap, I.V.; Kamat, P.V. Graphitic Design: Prospects of Graphene-Based Nanocomposites for Solar Energy Conversion, Storage, and Sensing. *Acc. Chem. Res.* **2013**, *46*, 2235–2243. [CrossRef]
10. Shen, J.; Liu, G.; Huang, K.; Jin, W.; Lee, K.R.; Xu, N. Membranes with Fast and Selective Gas-Transport Channels of Laminar Graphene Oxide for Efficient CO_2 Capture. *Angew. Chem.* **2015**, *54*, 578–582.
11. Srinivas, G.; Zhu, Y.; Piner, R.; Skipper, N.; Ellerby, M.; Ruoff, R. Synthesis of Graphene-like Nanosheets and Their Hydrogen Adsorption Capacity. *Carbon* **2010**, *48*, 630–635. [CrossRef]
12. Kim, H.W.; Yoon, H.W.; Yoon, S.-M.; Yoo, B.M.; Ahn, B.K.; Cho, Y.H.; Shin, H.J.; Yang, H.; Paik, U.; Kwon, S.; et al. Selective Gas Transport through Few-Layered Graphene and Graphene Oxide Membranes. *Science* **2013**, *342*, 91–95. [CrossRef] [PubMed]
13. Yoo, B.M.; Shin, J.E.; Lee, H.D.; Park, H.B. Graphene and Graphene Oxide Membranes for Gas Separation Applications. *Curr. Opin. Chem. Eng.* **2017**, *16*, 39–47. [CrossRef]
14. Srinivas, G.; Burress, J.; Yildirim, T. Graphene Oxide Derived Carbons (GODCs): Synthesis and Gas Adsorption Properties. *Energy Environ. Sci.* **2012**, *5*, 6453–6459. [CrossRef]
15. Dimiev, A.M.; Alemany, L.B.; Tour, J.M. Graphene Oxide. Origin of Acidity, its Instability in Water, and a New Dynamic Structural Model. *ACS Nano* **2013**, *7*, 576–588. [CrossRef] [PubMed]
16. Tamon, H.; Sone, T.; Okazaki, M. Control of Mesoporous Structure of Silica Aerogel Prepared from TMOS. *J. Colloid Interface Sci.* **1997**, *188*, 162–167. [CrossRef]
17. Georgakilas, V.; Otyepka, M.; Bourlinos, A.B.; Chandra, V.; Kim, N.; Kemp, K.C.; Hobza, P.; Zboril, R.; Kim, K.S. Functionalization of Graphene: Covalent and Non-Covalent Approaches, Derivatives and Applications. *Chem. Rev.* **2012**, *112*, 6156–6214. [CrossRef]
18. Georgakilas, V.; Tiwari, J.N.; Kemp, K.C.; Perman, J.A.; Bourlinos, A.B.; Kim, K.S.; Zboril, R. Noncovalent Functionalization of Graphene and Graphene Oxide for Energy Materials, Biosensing, Catalytic, and Biomedical Applications. *Chem. Rev.* **2016**, *116*, 5464–5519. [CrossRef]
19. Burress, J.W.; Gadipelli, S.; Ford, J.; Simmons, J.M.; Zhou, W.; Yildirim, T. Graphene Oxide Framework Materials: Theoretical Predictions and Experimental Results. *Angew. Chem.* **2010**, *49*, 8902–8904. [CrossRef]
20. Zhu, Y.; Murali, S.; Cai, W.; Li, X.; Suk, J.W.; Potts, J.R.; Ruoff, R.S. Graphene and Graphene Oxide: Synthesis, Properties, and Applications. *Adv. Mater.* **2010**, *22*, 3906–3924. [CrossRef]
21. Loh, K.P.; Bao, Q.; Eda, G.; Chhowalla, M. Graphene Oxide as a Chemically Tunable Platform for Optical Applications. *Nat. Chem.* **2010**, *2*, 1015–1021. [CrossRef] [PubMed]
22. Sui, Z.Y.; Cui, Y.; Zhu, J.H.; Han, B.H. Preparation of Three-Dimensional Graphene Oxide-Polyethylenimine Porous Materials as Dye and Gas Adsorbents. *ACS Appl. Mater. Interfaces* **2013**, *5*, 9172–9179. [CrossRef] [PubMed]
23. Chen, L.; Li, Y.; Du, Q.; Wang, Z.; Xia, Y.; Yedinak, E.; Lou, J.; Ci, L. High Performance Agar/Graphene Oxide Composite Aerogel for Methylene Blue Removal. *Carbohydr. Polym.* **2017**, *155*, 345–353. [CrossRef] [PubMed]

24. Fang, Q.; Chen, B. Self-Assembly of Graphene Oxide Aerogels by Layered Double Hydroxides Cross-Linking and Their Application in Water Purification. *J. Mater. Chem. A* **2014**, *2*, 8941–8951. [CrossRef]

25. Zhang, N.; Qiu, H.; Si, Y.; Wang, W.; Gao, J. Fabrication of Highly Porous Biodegradable Monoliths Strengthened by Graphene Oxide and Their Adsorption of Metal Ions. *Carbon* **2011**, *49*, 827–837. [CrossRef]

26. Ou, A.; Bo, I. Chitosan Hydrogels and Their Glutaraldehyde-Crosslinked Counterparts as Potential Drug Release and Tissue Engineering Systems—Synthesis, Characterization, Swelling Kinetics and Mechanism. *J. Phys. Chem. Biophys.* **2017**, *7*, 2161. [CrossRef]

27. Neufeld, M.J.; Lutzke, A.; Tapia, J.B.; Reynolds, M.M. Metal-Organic Framework/Chitosan Hybrid Materials Promote Nitric Oxide Release from S-Nitrosoglutathione in Aqueous Solution. *ACS Appl. Mater. Interfaces* **2017**, *9*, 5139–5148. [CrossRef]

28. Guo, X.; Qu, L.; Tian, M.; Zhu, S.; Zhang, X.; Tang, X.; Sun, K. Chitosan/Graphene Oxide Composite as an Effective Adsorbent for Reactive Red Dye Removal. *Water Environ. Res.* **2016**, *88*, 579–588. [CrossRef]

29. Yan, T.; Zhang, H.; Huang, D.; Feng, S.; Fujita, M.; Gao, X.-D. Chitosan-Functionalized Graphene Oxide as a Potential Immunoadjuvant. *Nanomaterials* **2017**, *7*, 59. [CrossRef]

30. Ahmed, J.; Mulla, M.; Arfat, Y.A.; Thai, T.L.A. Mechanical, Thermal, Structural and Barrier Properties of Crab Shell Chitosan/Graphene Oxide Composite Films. *Food Hydrocoll.* **2017**, *71*, 141–148. [CrossRef]

31. Zhang, D.; Yang, S.; Chen, Y.; Liu, S.; Zhao, H.; Gu, J. ^{60}Co γ-Ray Irradiation Crosslinking of Chitosan/Graphene Oxide Composite Film: Swelling, Thermal Stability, Mechanical, and Antibacterial Properties. *Polymers* **2018**, *10*, 294. [CrossRef] [PubMed]

32. Fan, H.; Wang, L.; Zhao, K.; Li, N.; Shi, Z.; Ge, Z.; Jin, Z. Fabrication, Mechanical Properties, and Biocompatibility of Graphene-Reinforced Chitosan Composites. *Biomacromolecules* **2010**, *11*, 2345–2351. [CrossRef] [PubMed]

33. Zuo, P.-P.; Feng, H.-F.; Xu, Z.-Z.; Zhang, L.-F.; Zhang, Y.-L.; Xia, W.; Zhang, W.-Q. Fabrication of Biocompatible and Mechanically Reinforced Graphene Oxide-Chitosan Nanocomposite Films. *Chem. Cent. J.* **2013**, *7*, 39–50. [CrossRef] [PubMed]

34. Park, S.; Lee, K.-S.; Bozoklu, G.; Cai, W.; Nguyen, S.T.; Ruoff, R.S. Graphene Oxide Papers Modified by Divalent Ions-Enhancing Mechanical Properties via Chemical Cross-Linking. *ACS Nano* **2008**, *2*, 572–578. [CrossRef] [PubMed]

35. Mathesh, M.; Liu, J.; Nam, N.D.; Lam, S.K.H.; Zheng, R.; Barrow, C.J.; Yang, W. Facile Synthesis of Graphene Oxide Hybrids Bridged by Copper Ions for Increased Conductivity. *J. Mater. Chem. C* **2013**, *1*, 3084–3090. [CrossRef]

36. Turgut, H.; Tian, Z.R.; Yu, F.; Zhou, W. Multivalent Cation Cross-Linking Suppresses Highly Energetic Graphene Oxide's Flammability. *J. Phys. Chem. C* **2017**, *121*, 5829–5835. [CrossRef]

37. Liu, R.; Gong, T.; Zhang, K.; Lee, C. Graphene Oxide Papers with High Water Adsorption Capacity for Air Dehumidification. *Sci. Rep.* **2017**, *7*, 9761–9770. [CrossRef]

38. Hummers, W.S.; Offeman, R.E. Preparation of Graphitic Oxide. *J. Am. Chem. Soc.* **1958**, *80*, 1339. [CrossRef]

39. Wang, X.; Jiao, L.; Sheng, K.; Li, C.; Dai, L.; Shi, G. Solution-Processable Graphene Nanomeshes with Controlled Pore Structures. *Sci. Rep.* **2013**, *3*, 1996–2001. [CrossRef]

40. Pelekani, C.; Snoeyink, V.L. Competitive Adsorption between Atrazine and Methylene Blue on Activated Carbon: The Importance of Pore Size Distribution. *Carbon* **2000**, *38*, 1423–1436. [CrossRef]

41. Inel, O.; Tumsek, F. The Measurement of Surface Areas of Some Silicates by Solution Adsorption. *Turk. J. Chem.* **2000**, *24*, 9–20.

42. Mohamed, M.H.; Dolatkhah, A.; Aboumourad, T.; Dehabadi, L.; Wilson, L.D. Investigation of Templated and Supported Polyaniline Adsorbent Materials. *RSC Adv.* **2015**, *5*, 6976–6984. [CrossRef]

43. Cieśla, J.; Sokołowska, Z.; Witkowska-Walczak, B.; Skic, K. Adsorption of Water Vapour and the Specific Surface Area of Arctic Zone Soils (Spitsbergen). *Int. Agrophysics* **2018**, *32*, 19–27. [CrossRef]

44. Sing, K. The Use of Nitrogen Adsorption for the Characterisation of Porous Materials. *Colloids Surf. Physicochem. Eng. Asp.* **2001**, *187*, 3–9. [CrossRef]

45. Brunauer, S.; Emmett, P.H.; Teller, E. Adsorption of Gases in Multimolecular Layers. *J. Am. Chem. Soc.* **1938**, *60*, 309–319. [CrossRef]

46. Sabzevari, M.; Wilson, L.D.; Cree, D.E. Mechanical properties of graphene oxide-based composite layered-materials. *Mater. Chem. Phys.* **2019**, *234*, 81–89. [CrossRef]

47. He, H.Y.; Riedl, T.; Lerf, A.; Klinowski, J. Solid-State NMR Studies of the Structure of Graphite Oxide. *J. Phys. Chem.* **1996**, *100*, 19954–19958. [CrossRef]

48. Mahaninia, M.H.; Wilson, L.D. Modular Cross-Linked Chitosan Beads with Calcium Doping for Enhanced Adsorptive Uptake of Organophosphate Anions. *Ind. Eng. Chem. Res.* **2016**, *55*, 11706–11715. [CrossRef]

49. Haouas, M.; Taulelle, F.; Martineau, C. Recent Advances in Application of ^{27}Al NMR Spectroscopy to Materials Science. *Prog. Nucl. Magn. Reson. Spectrosc.* **2016**, *94*, 11–36. [CrossRef]

50. Konkena, B.; Vasudevan, S. Understanding Aqueous Dispersibility of Graphene Oxide and Reduced Graphene Oxide through pK$_a$ Measurements. *J. Phys. Chem. Lett.* **2012**, *3*, 867–872. [CrossRef]

51. Chen, J.-T.; Fu, Y.-J.; An, Q.-F.; Lo, S.-C.; Huang, S.-H.; Hung, W.-S.; Hu, C.-C.; Lee, K.-R.; Lai, J.-Y. Tuning Nanostructure of Graphene Oxide/Polyelectrolyte LbL Assemblies by Controlling pH of GO Suspension to Fabricate Transparent and Super Gas Barrier Films. *Nanoscale* **2013**, *5*, 9081–9088. [CrossRef] [PubMed]

52. Emadi, F.; Amini, A.; Gholami, A.; ad Ghasemi, Y. Functionalized Graphene Oxide with Chitosan for Protein Nanocarriers to Protect against Enzymatic Cleavage and Retain Collagenase Activity. *Sci. Rep.* **2017**, *7*, 42258–42271. [CrossRef] [PubMed]

53. Samiey, B.; Tehrani, A.D. Study of Adsorption of Janus Green B and Methylene Blue on Nano-crystalline Cellulose. *J. Chin. Chem. Soc.* **2015**, *62*, 149–162. [CrossRef]

54. Jawad, A.H.; Razuan, R.; Appaturi, J.N.; Wilson, L.D. Adsorption and Mechanism Study for Methylene Blue Dye Removal with Carbonized Watermelon (*Citrullus lanatus*) Rind Prepared via One-Step Liquid Phase H$_2$SO$_4$ Activation. *Surf. Interfaces* **2019**, *16*, 76–84. [CrossRef]

55. Crini, G.; Badot, P.-M. Application of Chitosan, a Natural Aminopolysaccharide, for Dye Removal from Aqueous Solutions by Adsorption Processes Using Batch Studies: A Review of Recent Literature. *Prog. Polym. Sci.* **2008**, *33*, 399–447. [CrossRef]

56. Mohamed, M.H.; Udoetok, I.A.; Wilson, L.D.; Headley, J.V. Fractionation of Carboxylate Anions from Aqueous Solution Using Chitosan Cross-Linked Sorbent Materials. *RSC Adv.* **2015**, *5*, 82065–82077. [CrossRef]

57. Montes-Navajas, P.; Asenjo, N.G.; Corma, A. Surface Area Measurement of Graphene Oxide in Aqueous Solutions. *Langmuir* **2013**, *29*, 13443–13448. [CrossRef] [PubMed]

58. Sing, K.S.W. Reporting Physisorption Data for Gas/Solid Systems with Special Reference to the Determination of Surface Area and Porosity (Recommendations 1984). *Pure Appl. Chem.* **1985**, *54*, 2201–2218. [CrossRef]

59. Kumar, P.; Kim, K.-H.; Kwon, E.E.; Szulejko, J.E. Metal–Organic Frameworks for the Control and Management of Air Quality: Advances and Future Direction. *J. Mater. Chem. A.* **2016**, *4*, 345–361. [CrossRef]

60. Wilson, L.D.; Mohamed, M.H.; Headley, J.V. Surface Area and Pore Structure Properties of β-Cyclodextrin-Urethane Copolymer Materials. *J. Colloid Interface Sci.* **2011**, *357*, 215–222. [CrossRef]

61. Liu, B.; Salgado, S.; Maheshwari, V.; Liu, J. DNA Adsorbed on Graphene and Graphene Oxide: Fundamental Interactions, Desorption and Applications. *Curr. Opin. Coll. Interface Sci.* **2016**, *26*, 41–49.

62. Vaka, M.; ZheBian, M.; Nam, N.D. Highly Sensitive Pressure Sensor Based on Graphene Hybrids. *Arab. J. Chem.* **2018**. [CrossRef]

63. Kunde, G.B.; Yadav, G.D. Green Approach in the Sol–Gel Synthesis of Defect Free Unsupported Mesoporous Alumina Films. *Micro. Mesopor. Mater.* **2016**, *224*, 43–50. [CrossRef]

64. Savk, A.; Sen, B.; Demirkan, B.; Kuyuldar, E.; Aygun, A.; Salih, M. Graphene Oxide-Chitosan Furnished Monodisperse Platinum Nanoparticles as Importantly Competent and Reusable Nanosorbents for Methylene Blue Removal. In *Chitosan-Based Adsorbents for Wastewater Treatment*; Nasar, A., Ed.; Materials Research Foundations: Millersville, PA, USA, 2018; Volume 34, pp. 255–278.